Computational modelling of the semi-classical quantum vacuum in 3D

Zixin Zhang

zixin.zhang@physics.ox.ac.uk

University of Oxford

Ramy Aboushelbaya

University of Oxford

Rui Torres

https://orcid.org/0000-0002-9182-0228

Thomas Grismayer

Instituto Tecnico Superior (Lisbon University) https://orcid.org/0000-0002-0045-389X

Iustin Ouatu

Elliott Denis

Abigail James

Robin Timmis

University of Oxford https://orcid.org/0000-0002-2241-9633

Marko von der Leyen

Peter Norreys

University of Oxford https://orcid.org/0000-0002-5539-9464

Luis Silva

Instituto Superior Tecnico https://orcid.org/0000-0003-2906-924X

Article

Keywords:

Posted Date: November 8th, 2024

DOI: https://doi.org/10.21203/rs.3.rs-5305075/v1

Additional Declarations: There is **NO** Competing Interest.

Computational modelling of the semi-classical quantum vacuum in 3D

Z. Zhang,* R. Aboushelbaya, I. Ouatu, E. Denis, A. James, R. J. L. Timmis, M. W. von der Leyen, and P. A. Norreys†
Department of Physics, Atomic and Laser Physics sub-Department,
University of Oxford, Clarendon Laboratory, Parks Road, Oxford OX1 3PU, UK.

R. Torres, T. Grismayer, and L. O. Silva
GoLP/Instituto de Plasmas e Fusão Nuclear, Instituto Superior Técnico,
Universidade de Lisboa, 1049-001 Lisbon, Portugal
(Dated: October 18, 2024)

The commissioning of multi-Petawatt laser systems is gathering pace around the world, promising unparalleled access to ultra-high electromagnetic fields for fundamental Physics studies. Here, we present the first three-dimensional simulation results of two quantum vacuum effects using a semi-classical numerical solver for the Heisenberg-Euler Lagrangian. The simulation model is benchmarked against vacuum birefringence analytical results using counter-propagating probe and pump pulses. Simulations of both plane-wave and Gaussian pulses show results consistent with theoretical predictions. The solver is then applied to four-wave mixing using three realistic Gaussian pulses for the first time. First results of the polarisation and power of the output pulse and the number of photons obtained from the interaction are obtained and compared with theory. The output power and polarisation dependence on input polarisation is also investigated, and found to be consistent with the theoretical predictions.

I. INTRODUCTION

Quantum electrodynamics (QED) is one of the most fundamental and well-tested theories in Physics, validated by numerous precision tests [1–3]. One of the groundbreaking predictions of QED is on the nature of the vacuum, which is classically viewed as an empty space with no particles and zero energy. The quantum vacuum state is filled with virtual electron and positron pairs, and energy fluctuations. The presence of these virtual particles creates non-linearities in vacuum that interact with high power laser pulses travelling through, altering their properties. Examples of these interactions include vacuum birefringence [4–15], four-wave mixing [16–24], photon splitting and merging [25–29], and quantum reflections [30].

There have been various indirect tests for photon-photon scattering, the underlying reaction for the above QED effects. These include the inelastic scattering experiment at Stanford University (1997) colliding an electron beam with terawatt laser pulses [31], scattering of virtual photons at CERN using relativistic heavy-ion collisions (2017) [32] and forward proton scattering in association with lepton pairs produced via photon fusion (2020) [33]. The advent of multi-petawatt lasers is able to bring us into a new regime of direct tests for real photon-photon scattering [34–36]. Currently, the Extreme Light Infrastructure (ELI) in Romania [37] is able to deliver two 10-PetaWatt (PW) laser beams along with a tunable gamma-ray beam. Amongst the near-future high-power lasers is the Vulcan 20-20 laser at the Central Laser Facility in the United Kingdom [38], which will produce a primary beam of 20 PW, as well as 8 beams with a combined energy of 20 kJ. The EP-OPAL project [39] at the University of Rochester in the United States plans on generating two beams, each of 25 PW, along with four OMEGA EP kilojoule beamlines. Photon-photon scattering via four-wave mixing has been selected as one of the flagship experiments to be conducted in future EP-OPAL facility [40]. Finally, the station of extreme light (SEL) [41] at Shanghai High repetition rate X-ray Free Laser and Extreme light facility (SHINE) in China is aiming at building a 100 PW beam with a focused electric field strength up to 10^{15} V/m. This laser is also designed to combine with an X-ray free laser (XFEL) for pump–probe experiments such as vacuum birefringence. Unlike previous experiments, purely laser-based experiments provide a clean source of photons without interactions from other particles, significantly reducing the experimental noise. These experiments will not only probe the quantum vacuum directly, but also provide tests for alternative theories such as Born-Infeld electrodynamics [42, 43], axions [44, 45] and millicharged particles [46].

While experimental conditions are increasingly promising with these up-coming facilities, current theoretical models are somewhat limited and lagging behind. Analytical results have, by necessity, used plane wave approximations with infinite spatial properties, which are clearly unrealistic for laser beam profiles that can be realised in the laboratory. Numerical effects of non-ideal pulses have been unexplored so far, particularly in the context of multiple beam interactions such as four-wave mixing. This informs the need for more precise computational simulations to provide benchmarks for future experimental designs and real data sets.

Existing quantum vacuum simulation toolkits include

* zixin.zhang@physics.ox.ac.uk
† Also at John Adams Institute for Accelerator Science, University of Oxford, Denys Wilkinson Building, Keble Road, Oxford OX1 3RH, United Kingdom.

HEWES by Lindner, Ölmez, and Ruhl [47], and the vacuum emission picture solver by Blinne, Gies, et al. [48]. HEWES adopts a fully semi-classical treatment for four-and six-photon processes, achieving high accuracy without requiring spatial or temporal interpolation. The vacuum emission picture solver treats quantum vacuum signature as signal photons. External fields are treated classically, while the emission amplitude of signal photons is calculated on a quantum level. It is less limited by grid resolution for ultra-short laser wavelengths, but does not account for self-induced quantum effects of the laser pulses or their back-reactions on the vacuum.

This paper builds on the work presented in [49] on a Heisenberg-Euler (HE) solver based on a modified Yee scheme and extends the solver from one and two dimensions to three dimensions for the first time. The solver evaluates and propagates the fields using non-linear Maxwell's equations with non-linearity source terms derived from the HE Lagrangian. The numerical stability and robustness of the solver have been thoroughly tested in lower dimensions. This approach is matrix-free numerical method, and is implemented as part of OSIRIS [50], a highly parallel and fully relativistic particle-in-cell (PIC) code that has been extensively benchmarked against high intensity laser-plasma interaction experiments, particularly those associated with laser-wakefield accelerators. The integration into OSIRIS allows for greater flexibility in simulating a wide range of quantum phenomena [51–53], both in vacuum and in the presence of particles, as will naturally arise in experiments.

In this paper, we incorporate the solver into the latest version of OSIRIS and aim to validate its robustness in three dimensions by benchmarking it against two quantum vacuum phenomena: vacuum birefringence and four-wave mixing.

This paper is organised as follows. In Section II, a brief overview of the theory underpinning the semi-classical definition of the quantum vacuum is provided, along with analytical results for the two phenomena considered. Section III provides an outline of the three-dimensional algorithm of the modified Yee scheme used in the new solver. A discussion of simulation results and comparisons to analytic theory are presented in Section IV. Section V summarises the results and concludes the article.

II. THEORY

QED in vacuum can be approximated by the HE Lagrangian [54, 55], non-linear in electric and magnetic fields, as expressed below in Gaussian units:

$$\mathcal{L} = \frac{1}{8\pi}\left(E^2 - B^2\right) + \frac{\xi}{8\pi}\left[\left(E^2 - B^2\right)^2 + 7\left(\mathbf{E}\cdot\mathbf{B}\right)^2\right], \quad (1)$$

where ξ is the non-linearity coupling parameter:

$$\xi = \frac{\hbar e^4}{45\pi m^4 c^7}. \quad (2)$$

This approximation holds under the conditions for fields $E \ll E_s$ and $\lambda \gg \lambda_c$, where $E_s = \frac{m_e^2 c^3}{e\hbar} \sim 10^{18}$ V/m is the Schwinger field, and $\lambda_c = \frac{h}{mc} \sim 10^{-12}$ m is the Compton wavelength [56]. All simulations presented in this paper have fields and wavelengths strictly within these limits.

A set of semi-classical non-linear Maxwell's equations can be derived from the Lagrangian [57]:

$$\nabla\cdot\mathbf{E} = -4\pi\nabla\cdot\mathbf{P}, \quad (3)$$

$$\nabla\times\mathbf{E} + \frac{1}{c}\frac{\partial\mathbf{B}}{\partial t} = 0, \quad (4)$$

$$\nabla\cdot\mathbf{B} = 0, \quad (5)$$

$$\nabla\times\mathbf{B} - \frac{1}{c}\frac{\partial\mathbf{E}}{\partial t} = 4\pi\frac{1}{c}\frac{\partial\mathbf{P}}{\partial t} + 4\pi\nabla\times\mathbf{M}, \quad (6)$$

where we define an effective polarisation $\mathbf{P}$ and magnetisation of the vacuum $\mathbf{M}$ as:

$$\mathbf{P} = \frac{\xi}{4\pi}\left[2\left(E^2 - B^2\right)\mathbf{E} + 7(\mathbf{E}\cdot\mathbf{B})\mathbf{B}\right], \quad (7)$$

$$\mathbf{M} = \frac{\xi}{4\pi}\left[-2\left(E^2 - B^2\right)\mathbf{B} + 7(\mathbf{E}\cdot\mathbf{B})\mathbf{E}\right]. \quad (8)$$

We can also derive the non-linear wave equation

$$\left(\frac{\partial^2}{\partial t^2} - c^2\nabla^2\right)\mathbf{E} = 4\pi c^2\left[\nabla(\nabla\cdot\mathbf{P}) - \partial_t\left(\partial_t\mathbf{P} + \nabla\times\mathbf{M}\right)\right] \quad . \quad (9)$$

Under this formulation, the vacuum possesses non-linear electromagnetic properties and interacts with laser pulses propagating through it. The two effects of interest in this paper are vacuum birefringence and four-wave mixing. The following sections present an overview of the analytical solutions for the two effects, which will be compared to simulation results.

A. Vacuum birefringence

In vacuum birefringence [4–15], a probe pulse travelling through a strong electromagnetic background will experience a change in its refractive indices along different polarisations. Specifically, the difference in refractive indices leads to dephasing between the different polarisation components. A linearly polarised probe pulse will thus gain a small ellipticity in its polarisation after passing through the strong background. In our simulations, the strong field is provided by an ultra-intense pump pulse, and we extract the birefringence from a probe pulse that passes through the pump pulse [49, 58]. The two pulses will be counter-propagating along the $\hat{\mathbf{x}}$-axis.

We consider two scenarios. In the first scenario, both the pump and probe pulses are plane waves with a Gaussian temporal profile [58]:

$$\mathbf{E}_{0,p}(\mathbf{r},t) = \bar{\mathbf{E}}_{0,p}\cos(k_{0,p}x \pm \omega_{0,p}t)\exp\left(-\frac{(x \pm ct)^2}{2\sigma_{0,p}^2}\right), \quad (10)$$

where $\mathbf{E}_{0,p}$ is the pump and probe pulse profile, $\bar{\mathbf{E}}_{0,p}$ is the amplitude of the respective pulses, $k_{0,p}$ and $\omega_{0,p}$ are their wave-numbers and frequencies, and $\sigma_{0,p}$ are their longitudinal duration.

In the second scenario, both are finite-width Gaussian beams under the paraxial approximation:

$$\mathbf{E}_{0,p}(\mathbf{r},t) = \bar{\mathbf{E}}_{0,p}\exp\left(-\frac{y^2+z^2}{2W_{0,p}^2}\right)\cos(k_{0,p}x+\omega_{0,p}t) \times \exp\left(-\frac{(x\pm ct)^2}{2\sigma_{0,p}^2}\right), \tag{11}$$

where $W_{0,p}$ are the transverse widths of the two pulses. In both cases, $\bar{E}_0 \gg \bar{E}_p$, such that the birefringent effect created from the probe pulse can be considered negligible. For a probe pulse that is initially linearly polarised at θ, it will acquire a phase difference between its two components along $\hat{\mathbf{y}}$ and $\hat{\mathbf{z}}$ after the interaction:

$$\mathbf{E}_p(x,t) = \frac{\overline{E}_p}{2}\exp(-i\omega t)\exp(ik'x)\left[\cos(\theta)\exp(-i\delta)\mathbf{e}_y + \sin(\theta)\mathbf{e}_z\right] + \text{c.c.}, \tag{12}$$

where k' is the wave-number altered by the non-linear vacuum, and δ is the ellipticity given by [58, 59]

$$\delta = 12\pi\sqrt{\pi}\xi\overline{E_0^2}k_p\sigma_0 \tag{13}$$

for plane waves, and

$$\delta(y,z) = \frac{3}{2}\pi\sqrt{\pi}\xi\overline{E_0^2}\exp\left(-\frac{y^2+z^2}{W_0^2}\right)k_p\sigma_0 \tag{14}$$

for paraxial Gaussian beams. c.c. denotes the complex conjugate of the first term.

B. Four-wave mixing

We consider three input plane waves with frequencies and wavevectors $(\omega_i, \mathbf{k_i})$. An output beam whose four-wavevector satisfies the conservation of energy and momentum will be generated such that: [60].

$$\mathbf{k_1}+\mathbf{k_2} = \mathbf{k_3}+\mathbf{k_4}, \tag{15}$$

$$\omega_1+\omega_2 = \omega_3+\omega_4. \tag{16}$$

We assign the angles ϕ_i and γ_i to each field, where ϕ_i is defined as the angle $\mathbf{k}$ makes with the x-axis, and γ_i is the angle of polarisation from the z-axis, such that:

$$\mathbf{k_i} = k_i\cos\phi_i\hat{\mathbf{x}} + k_i\sin\phi_i\hat{\mathbf{y}}, \tag{17}$$

$$\mathbf{E_i}(\mathbf{r},t) = E_i(\mathbf{r},t)\left[\sin\gamma_i\sin\phi_i\hat{\mathbf{x}} - \sin\gamma_i\cos\phi_i\hat{\mathbf{y}} + \cos\gamma_i\hat{\mathbf{z}}\right]. \tag{18}$$

Incoming beams are approximated as top-hat beams with length L, width and height b ($L > b$). It is further approximated that during the interaction process, the pulses interact in a cubic region with volume b^3, and edge-effects are negligible. The output electric field then takes the form [60]

$$\mathbf{E}_{out}(\mathbf{r},t) = E_0(r,\theta,\phi)\cos(k_4 r-\omega_4 t+\delta)\mathbf{G}_{2d}, \tag{19}$$

where

$$E_0(r,\theta,\phi) = \frac{1}{4\pi\epsilon_0}\frac{8\xi}{k_4\pi r}\frac{\sin\left(k_4\frac{b}{2}(\cos\phi_4-\cos\phi\sin\theta)\right)}{\cos\phi_4-\cos\phi\sin\theta} \frac{\sin\left(k_4\frac{b}{2}(\sin\phi_4-\sin\phi\sin\theta)\right)}{\sin\phi_4-\sin\phi\sin\theta}\frac{\sin\left(k_4\frac{b}{2}\cos\theta\right)}{\cos\theta} G_{2d}\sqrt{\frac{2P_1}{c\epsilon_0}}\sqrt{\frac{2P_2}{c\epsilon_0}}\sqrt{\frac{2P_3}{c\epsilon_0}}. \tag{20}$$

r, θ and ϕ are conventional spherical coordinates, with the origin at the interaction centre. G_{2d} is a geometric factor that depends on the interaction geometry and polarisation of input pulses. A full expression for G_{2d} can be found in appendix A.

The output power can be calculated by integrating the intensity over a spherical shell, which gives

$$P_{\text{out}} = \frac{4\xi^2}{c^2\epsilon_0^2}\left(\frac{1}{\lambda_4}\right)^4 G_{2d}^2\alpha^2\left(\frac{L}{b}\right)^4 P_1P_2P_3, \tag{21}$$

with α^2 given by [17]

$$\alpha^2 = \frac{64}{k_4^4b^6}\int_0^{2\pi}\int_0^{\pi}\frac{\sin^2\left[k_4bf(\theta,\phi)/2\right]\sin^2\left[k_4bg(\theta,\phi)/2\right]}{f^2(\theta,\phi)g^2(\theta,\phi)} \times \frac{\sin^2\left[k_4\frac{b}{2}\cos\theta\right]}{\cos^2\theta}\sin\theta\,d\theta\,d\phi, \tag{22}$$

where $f(\theta,\phi) = 1-\cos\phi\sin\theta$ and $g(\theta,\phi) = \sin\phi\sin\theta$. $P_{1,2,3}$ represent the power of the input pulses. The expeceted number of photons obtained per shot (N_{out}) is calculated by multiplying the power by the time duration and dividing by the output photon energy:

$$N_{\text{out}} = \frac{4\xi^2}{c^2\epsilon_0^2\hbar}\left(\frac{1}{\lambda_4}\right)^3 G_{2d}^2\alpha^2\frac{L^5}{b^4}P_1P_2P_3. \tag{23}$$

We will use Eq. (13), (14), (19), (21), (23) to benchmark our numerical solver.

III. SEMI-CLASSICAL QED SOLVER

The Yee scheme [61, 62] is a widely used solver for Maxwell's equations, wherein the electric and magnetic fields are computed on a staggered grid (Fig. (1)). To address the non-linearities in the modified Maxwell's equations, our solver employs a modified Yee scheme [49](Fig. (2)). At each time step t_n:

1. The standard Yee scheme, based on the original Maxwell's equations in absence of vacuum non-linearities, is carried out to compute the electric and magnetic fields at staggered locations at t_{n+1}.

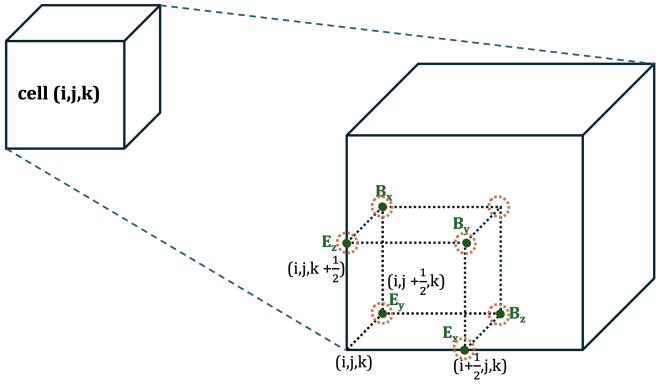

FIG. 1: Positions where electric and magnetic fields are evaluated in the Yee scheme in 3D. Positions for interpolation and calculation of invariants are represented by dashed circles in orange.

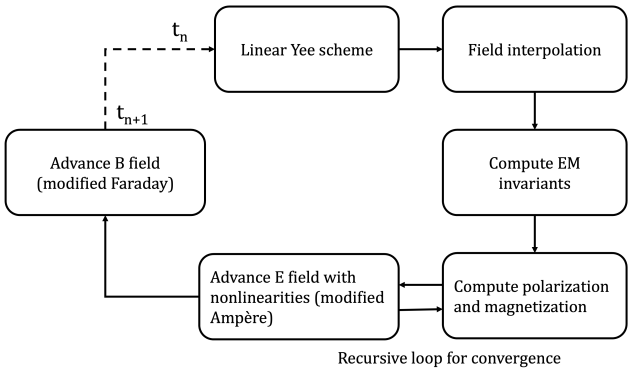

FIG. 2: Iterative loop in the modified Yee scheme.

2. The field values are interpolated to all grid locations.

3. The two electromagnetic invariants, $E^2 - B^2$ and $\mathbf{E} \cdot \mathbf{B}$ are calculated at all grid locations at t_{n+1}.

4. The effective polarisation (Eq. (7)) and magnetisation (Eq. (8)), are calculated at all grid locations at t_{n+1}.

5. The electric field at t_{n+1} is then re-evaluated using the modified Ampere's Law (Eq. (4)).

6. The updated electric field is used to revise the polarisation (Eq. (7)) and magnetisation terms (Eq. (8)), which in turn update the electric field (Eq. (6)). This iterative process continues until convergence to the desired accuracy is achieved.

7. The magnetic field at t_{n+1} is then re-calculated using the modified Faraday's Law (Eq. (6))

This scheme has the important advantange that it can be straightforwardly incorporated into the electromagnetic solver in PIC code, and allows the calculation of semi-classical quantum vacuum effects in the existing PIC code algorithm without significant modifications. We have upgraded the solver to be compatible with the latest version of OSIRIS, which supports new features such as pulse propagation at an angle [63], and benefits from a shorter run-time. For instance, the three-dimensional simulation of vacuum birefringence as introduced below, where two plane-wave pulses propagate through the vacuum, took approximately 0.5 hour to complete without quantum effects, and 15 hours with the addition of the quantum vacuum solver., for the same computational resources. The simulations of four-wave mixing took 0.75 and 3.4 hours without and with the solver. The reasonable run-time allows for higher flexibility in running multiple simulations, for example when carrying out parameter scans.

IV. RESULTS

A. Vacuum birefringence

The stability and accuracy of the solver in 1D and 2D have been validated in [49]. Here we extend the benchmarking to vacuum birefringence in 3D for the two scenarios outlined in Eq. (10) and Eq. (11). To enhance the non-linear effects, we have artificially increased the value of the non-linearity coupling parameter ξ in Eq. (7) and Eq. (8) from 3.28×10^{-51} to 1.08×10^{-44}. We note that this adjustment only re-scales the results without introducing additional physical effects.All diagnostic calculations are performed using $\mathbf{E}$ and $\mathbf{B}$ fields interpolated to the grid center.

The standard counter-propagating setup, shown in Fig. 3, consists of an optical pump pulse and an X-ray probe pulse. The two pulses share the same focal spot, duration and beam width, and fully overlap at the focal spot. The pulse parameters for the plane-wave scenario are detailed in Table I. The ellipticity value is measured from the polarisation plane of the probe pulse at a fixed location. Results for the ellipticity obtained in the plane-wave case are plotted as a ratio of the theoretical prediction (Eq. (13)) across the transverse plane, as shown in Fig.4(a). The maximum deviation from theory is 3.1%, demonstrating excellent agreement. There is a variation in the ratio within a range of 4.3% across the transverse plane, demonstrating the robustness of the solver across the $\hat{\mathbf{y}}$-$\hat{\mathbf{z}}$ plane.

For the Gaussian setup (Fig. 3(b)), both pulses have the same transverse Gaussian profile, with simulation parameters presented in Table II. The ellipticity is expected

TABLE I: Input parameters for pump and probe pulse in plane-wave scenario.

Pulse	λ (nm)	E_0 (V/m)	σ (fs)
Pump	1000	8.6×10^{14}	2.1
Probe	10	3.2×10^{12}	2.12

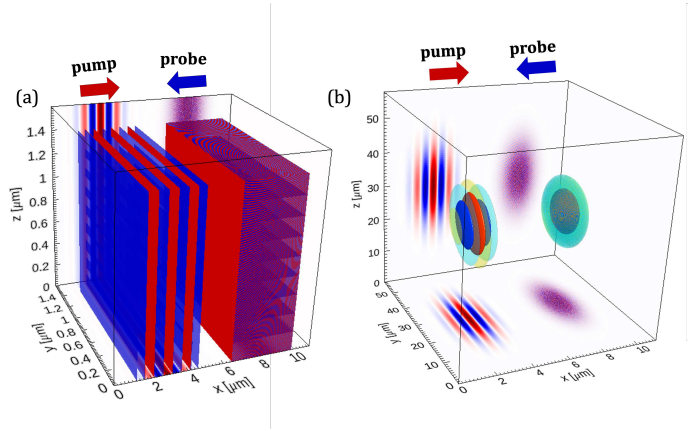

FIG. 3: Vacuum birefringence counter-propagating probe and pump setup in 3D: (a) both probe and pump pulses are plane waves. (b) both are Gaussian beams.

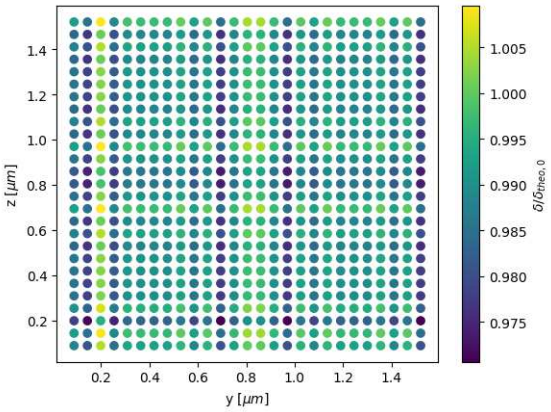

FIG. 4: Normalised ellipticity, δ/δ_{theo}, across the transverse plane of probe pulse for plane-wave scenario. Maximum deviation from the theoretical prediction is 3.1%, with a variation of 4.3% across the plane.

to mirror the Gaussian profile of the pump pulse across the $\hat{\mathbf{y}}$-$\hat{\mathbf{z}}$ plane, as shown in Fig. 5. Comparison with theory is shown in slices along the central $\hat{\mathbf{y}}$ and $\hat{\mathbf{z}}$ axes. The deviation from theory at the peak of the Gaussian is 2.1% and is found to be resolution dependent. Increasing the y-z plane resolution by 1.8 times reduces the deviation to 1.7%. The deviation from analytical predictions for both scenarios is consistent with previous deviations obtained in past literature when the solver was benchmarked in

TABLE II: Input parameters for pump and probe pulse in Gaussian scenario.

Pulse	λ (nm)	E_0 (V/m)	σ (fs)	W (μm)
Pump	1000	8.6×10^{14}	2.1	6.75
Probe	10	3.2×10^{12}	2.1	6.75

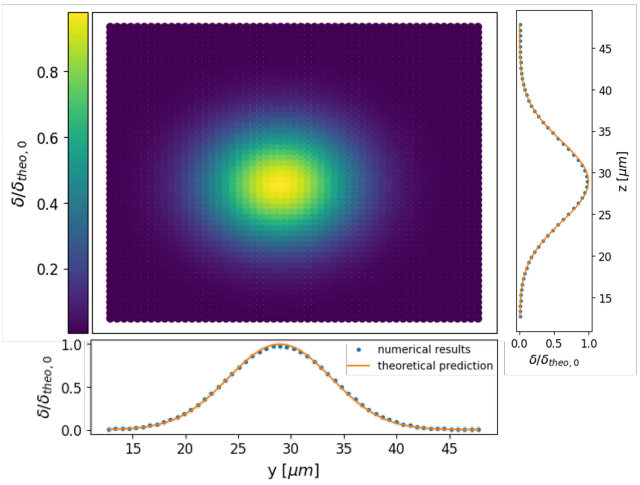

FIG. 5: Normalised ellipticity across transverse plane for the Gaussian scenario. Slices are taken along $\hat{\mathbf{y}}$ and $\hat{\mathbf{z}}$-axis at central $\hat{\mathbf{y}}$ and $\hat{\mathbf{z}}$ locations (30 μm), demonstrating high agreement with theory. Deviation from theoretical value of the peak ellipticity is 2.1%.

two dimensions [58], validating the continued accuracy of the solver when extended to three dimensions.

B. Four-wave mixing

The particular geometry studied here is

$$\begin{cases} \mathbf{k_1} = k\,\hat{\mathbf{x}} - \sqrt{3}k\,\hat{\mathbf{y}} \\ \mathbf{k_2} = k\,\hat{\mathbf{x}} + \sqrt{3}k\,\hat{\mathbf{y}} \\ \mathbf{k_3} = -k\,\hat{\mathbf{x}} \\ \mathbf{k_4} = -3k\,\hat{\mathbf{x}} \end{cases}, \tag{24}$$

as shown by Fig. 6, reproducing the setup studied theoretically in [17, 22]. The output beam is well-separated from the three incoming beams, making detection straightforward. This geometry also yields a reasonable number of photons compared to other potential setups [60].

TABLE III: Input parameters for pump and probe pulse in plane-wave scenario.

$\lambda_1(\mu m)$	$\lambda_2(\mu m)$	$\lambda_3(\mu m)$	$\lambda_4(\mu m)$
0.5	0.5	1	0.33
E_0 (V/m)	P_0(PW)	σ(fs)	$W(\mu m)$
6.4×10^{14}	13.9	13.3	2.8

The plane waves considered in theory are physically unrealistic and offer limited insight for future experiments. Therefore, in our simulation, all three beams

have realistic Gaussian profiles longitudinally and transversely. The input beams each have a wavelength of 0.5 μm (λ_1 and λ_2) and 1 μm (λ_3). They share the same electric field strength, pulse duration and beam width, as shown by Table III. This specific interaction geometry will yield a third harmonic output pulse, with a wavelength of 0.3 μm. We start with the simplest polarisation configuration: all three input beams are polarised along the $\hat{\mathbf{z}}$-axis. Fig. 7 shows the interaction at three different stages: initial stage ($\omega\mathbf{t} = \mathbf{0}$) where the interaction has not started, interaction stage (ωt = 100) where the three pulses fully overlap, and final stage (ωt = 200) where the interaction is complete.

Fig. 8 shows the resulting Fast Fourier Transforms (FFT) in the $\hat{\mathbf{x}}$-$\hat{\mathbf{y}}$ plane at the three stages, which allow us to identify the range of harmonics produced in the simulation. The six highest-intensity harmonics at locations $(k_x, k_y) = (\pm\, k_0, 0)$ and $(\pm\, k_0, \pm\sqrt{3}\, k_0)$ represent the three input beams. Unlike plane waves in theory with an infinitely sharp peak at single frequencies, the harmonics in the simulation are smeared out around the central frequencies due to finite pulse sizes. The white strips along k_x and k_y come from imperfections in pulse propagation in the simulation, but because of their much lower intensity, they create little effect on the third harmonic we wish to extract. From Fig.8(a) we can see the harmonics at $(\pm 3\, k_0, 0)$ and $(\pm 3\, k_0, \pm 3\sqrt{3}\, k_0)$ arising due to self-interaction of the input beams [58]. We note that self-interaction occurs only in non-plane-wave pulses, where the curvature of the wave fronts induces photon-photon scattering within the pulse itself. This is hence not captured in the plane-wave theory described in Section II B. The harmonics produced from the three-beam interaction are presented by Fig.8 (b). From Eq. (9), we can see that the output electric field includes the frequency components present in the non-linear source term, which scales as E^3. Substituting the input field as:

$$\mathbf{E}(\mathbf{r},t) = \Big(\mathbf{E}_1(\mathbf{r},t)e^{-ikx} + \mathbf{E}_2(\mathbf{r},t)e^{ik(x+\sqrt{3}y)} + \mathbf{E}_3(\mathbf{r},t)e^{ik(x-\sqrt{3}y)}\Big) + c.c. \qquad (25)$$

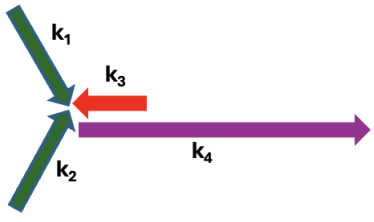

FIG. 6: A schematic view of the interaction geometry in the simulation, where the wave-vectors of all four beams lie on the $\hat{\mathbf{x}} - \hat{\mathbf{y}}$ plane. The four beams have a wavelength of 0.5 μm(λ_1 and λ_2), 1 μm(λ_3) and 0.3 μm(λ_4).

into Eq. (9) gives a range of harmonics including $(\pm k_0, \pm 2\sqrt{3}\, k_0)(\pm k_0, \pm 3\sqrt{3}\, k_0)(\pm 3k_0, 0)$,$(\pm 3k_0, \pm\sqrt{3}\, k_0)$ and $(\pm 3k_0, \pm 2\sqrt{3}\, k_0)$. However, approaching the end of the simulation, most of these harmonics are found to be non-propagating and fade away, while the amplitude of the third harmonic stays relatively constant, making it easily distinguishable from the other frequency components. These plots align with the principle of the four-wave mixing experiment, which is used to stimulate the generation of this particular harmonic.

The output pulse is extracted by placing a frequency filter around ω_4, and further filtering out the positive k mode. The final output pulse is shown in Fig. 8(b), also exhibiting a Gaussian-like profile, and polarised along the $\hat{\mathbf{z}}$-axis, consistent with the theoretical predictions given by appendix A. The output pulse is shorter than the input ones, with $\sigma \sim 8.7$ fs. It is also smaller in size and astigmatic, with $W \sim 1.8$ μm along the $\hat{\mathbf{y}}$-axis, and 2.2 μm along the $\hat{\mathbf{z}}$-axis. The astigmatism comes from the asymmetry the interaction geometry. As the wave-vectors of the primary beams lie on the x-y plane, when the beams approach each other at oblique incidence, they are able to overlap fully along the $\hat{\mathbf{z}}$-axis, but only partially along the $\hat{\mathbf{y}}$-axis. This leads to a smaller size of the output pulse along the $\hat{\mathbf{y}}$-axis than along the $\hat{\mathbf{z}}$-axis. Astigmatism has been ignored in previous analytical calculations, where the interaction region is simplified as cubic.

To compare with analytical results, we matched the input power of the plane waves used in theoretical calculations with the peak power of Gaussian pulses in the simulations. The full length and width of the plane waves are approximated by 4σ of the Gaussian pulses longitudinally and transversely, respectively 15.9 and 11.3 μm. We compare the peak electric field, peak power of the output pulse and the total number of photons emitted per interaction with the theoretical predictions. As we can see from (Eq. (19,21,23)), the output electric field has a 1/r dependence, while output power and energy are independent of detector distance. Given the difference in pulse shapes between theory and simulation, we expect reasonable discrepancies between the two. Specifically, because of the peak power matching, we expect theoretical results to be higher than simulation results. An additional contribution to the difference between the two is the simplification of the interaction region in analytical calculations. The theoretical model [60] approximates the region as cubic, while from Fig. 7(b) it could be seen that the region consistently deviates from cubic.

Fig. 10 represents the ratio of theoretical to simulation results for the respective quantities against the detector distance from the interaction point. On average, there is a factor of 1.5 difference between theory and simulation results for peak power of output pulse, while for photon number the ratio reaches 9.8. The larger discrepancy in photon number is again justified by the peak power matching, since theory assumes plane-wave inputs with a constant power, whereas the power of Gaussian pulses

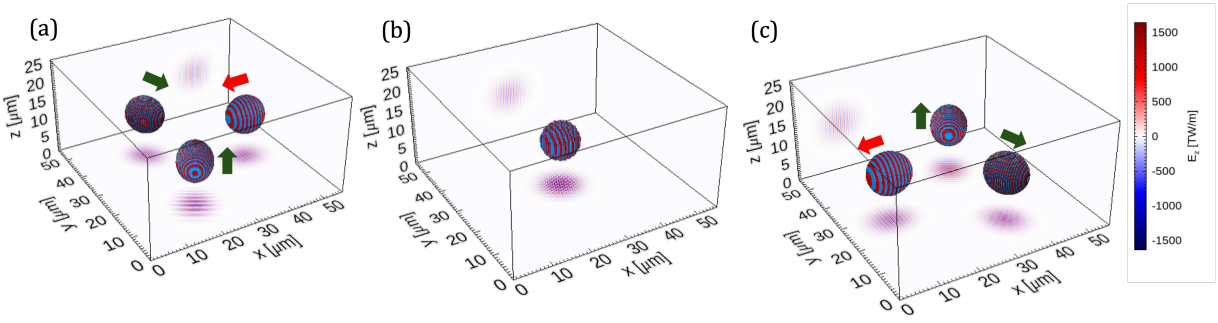

FIG. 7: Three-dimensional setup of four-wave mixing at three stages, ωt= (a) 0, (b) 100 and (c) 200.

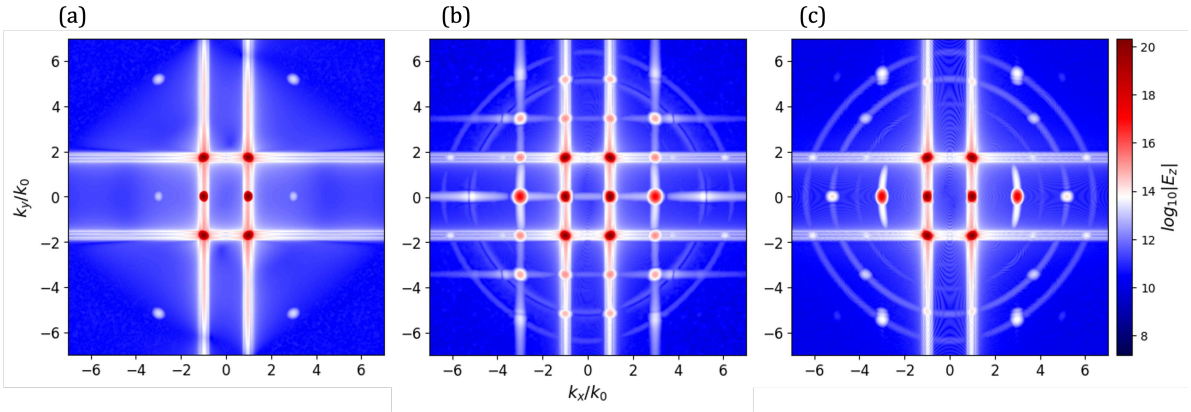

FIG. 8: FFT in the x-y plane at ωt= (a) 1, (b) 100 and (c) 200, where ω is the fundamental frequency. k values are normalised by the fundamental frequency. The initial harmonics in (a) are produced from self-interaction of the input beams. Harmonics produced from four-wave mixing are presented at (b), consistent with simple harmonic analysis. The third harmonics at $(\pm 3\,k_0, 0)$ remain the highest intensity amongst all higher harmonics throughout the interaction.

falls off rapidly away from the peak position. The biggest variation is found in the peak electric field ratio, which drops progressively with detector distance. This is because the analytical expression (Eq. (19)) relies on the assumption that the observer distance is much greater than the interaction length ($r \gg L$) [60], whereas the range of length scales we investigated are of the same order as the interaction length. The dropping discrepancy as the detector is placed further away is also justified by this assumption. This marks the success of the simulation to produce more accurate results close to the interaction point than analytical predictions. The ratios of power and photon number are also analysed at various distances from the interaction point to assess the consistency of the simulation results. The output power shows a maximum variation of 4.4% in a range of 12 μm, while the number of photons varies by up to 2.9% in 6 μm, further demonstrating the robustness of the solver to propagate the output pulse in space and time without diffraction effects.

The comparisons indicate that the simulation captures the results at close distances to the interaction point including finite pulse effects, which is challenging for analytical solutions. To further validate the reliability of the simulation, we investigated the dependence of normalised power and polarisation of the output pulse as a function of the polarisation angle of the three input beams, which are independent of input beam profile, and compared them with theoretical predictions. Nine simulations with the same interaction geometry were run while varying the polarisation angle γ of the three input pulses. Fig. 11 shows the normalised power and polarisation of the output pulse from simulation results and theory. The simulation results closely match the theoretical predictions for the angles tested, validating the accuracy of the solver when applied to a novel quantum phenomenon and field configuration.

V. CONCLUSIONS

In this paper, we introduced a semi-classical three-dimensional solver for quantum vacuum effects, based on the Heisenberg-Euler Lagrangian. The solver operates on

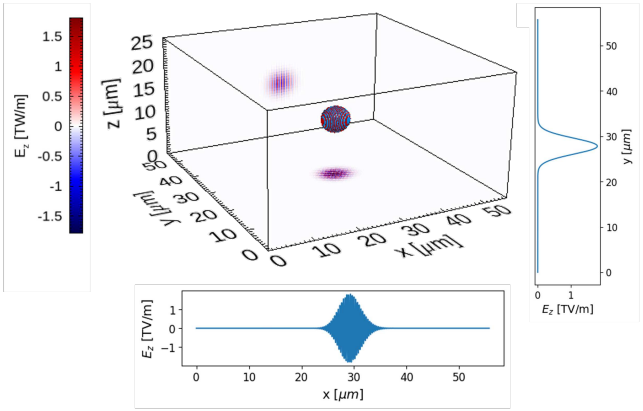

FIG. 9: Resulting output pulse. Electric field is shown in Terravolts/metre. Slices along $\hat{\mathbf{x}}$ and $\hat{\mathbf{y}}$ axes are taken along the centre of the simulation. The output pulse is smaller than input pulses and astigmatic, due to the asymmetry of the interaction region.

a modified Yee scheme and is integrated into the larger PIC framework OSIRIS. We demonstrated the accuracy and robustness of the HE QED solver in three dimensions by applying it to two quantum vacuum phenomena: vacuum birefringence, and, for the first time, four-wave mixing. In vacuum birefringence, we simulated two scenarios:

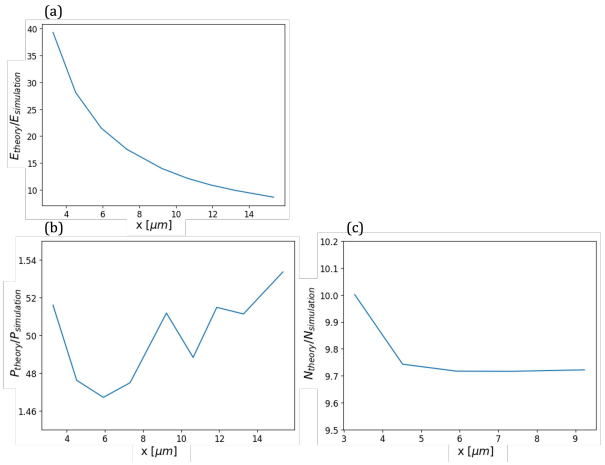

FIG. 10: Ratio of analytical results to simulation results for (a) peak electric field, (b) output power, (c) total number of photons against distance of detector from the interaction point. For all three quantities analytical predictions are consistently higher than simulation results because of power matching. Due to the assumption in the derivation for electric field [60] that the detector distance is far greater than interaction length, analytical results for electric field overshoots close to the interaction point. Ratio of power and photon number remain relatively constant with distance.

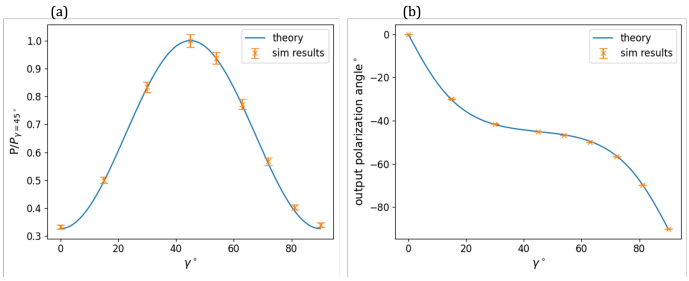

FIG. 11: The solver is benchmarked against four-wave mixing theory by investigating (a) normalized power and (b) polarisation angle of the output pulse as a function of the polarisation angle of input pulses. All datapoints align well with theory within error bars.

plane-wave and Gaussian laser input pulses. The results were benchmarked against theoretical predictions, verifying the accuracy of the solver. We also show the first ever simulation results of four-wave mixing in 3D employing realistic Gaussian beams. The theoretically predicted third harmonic output pulse is observed in our simulations. Simulation results have been benchmarked with theory by examining the dependence of signal strength and polarisation on input polarisations. Results from a set of simulations are highly consistent with theory, once again verifying the precision of the solver. Comparison of the output electric field, power and number of photons obtained from the interaction with analytical results also demonstrate the solver's capability to simulate realistic pulse shapes that analytical methods cannot easily address. The application of the solver in the two scenarios marks its versatility in investigating different quantum vacuum phenomena. Looking ahead, the solver could be applied to studying interactions of novel pulse shapes, including Laguerre-Gaussian beams [64] and tightly focused beams. The simulation results will complement existing theoretical work and provide benchmarks for future high-power laser experiments. Additionally, it opens up the possibility of investigating QED effects in the presence of particles. For example, in future four-wave mixing experiments, the solver could place initial estimates of noise levels from Compton scattering, thus opening the way to full-scale modelling of upcoming photon-photon scattering experiments with optical

ACKNOWLEDGMENTS

This work was supported by the Oxford-ShanghaiTech collaboration agreement project and the John Adams Institute grant ST/V001655/1, and partially supported by FCT (Foundation for Science and Technology, Portugal) under the project X-MASER No. 2022.02230.PTDC. Z. Z acknowledges support from the Clarendon Scholarship scheme, and useful discussions with R Almeida, P Bilbao and T Silva. The simulations were performed on

computing resources provided by UKRI-STFC Scientific Computing Department's SCARF cluster.

COMPETING INTERESTS

The authors declare no competing interests.

AUTHOR CONTRIBUTIONS

Z.Z. updated the solver to OSIRIS 4.0, produced the simulation results and wrote the manuscript. R.T.and T.G. developed the original solver and benchmarking in two dimensions, and provided vital discussions for vacuum birefringence. R.A. supervised the project day-to-day. P.A.N. and L.O.S were the overall supervisors for the project. All the authors discussed the results and reviewed the manuscript.

DATA AVAILABILITY

Data sets generated during the current study are available from the corresponding author on reasonable request.

Appendix A: 2D geometric factor

The geometric factor incorporates all the dependences on interaction geometry and polarisation in four-wave mixing, and are calculated theoretically as [60]:

$$
\begin{aligned}
\mathbf{G}_{2d} = \frac{1}{2}\Bigg\{ & \left[\frac{7}{4}\cos\gamma_3\sin(\gamma_1+\gamma_2) - \sin\gamma_3\cos(\gamma_1+\gamma_2)\right] \\
& \times \left[\sin(\phi_3-\phi_4)\cos\phi_4 - (\sin\phi_3 - \sin\phi_4)\right]\sin^2\left(\frac{\phi_1-\phi_2}{2}\right) \\
& + \left[\frac{7}{4}\cos\gamma_2\sin(\gamma_1+\gamma_3) - \sin\gamma_2\cos(\gamma_1+\gamma_3)\right] \\
& \times \left[\sin(\phi_2-\phi_4)\cos\phi_4 - (\sin\phi_2 - \sin\phi_4)\right]\sin^2\left(\frac{\phi_1-\phi_3}{2}\right) \\
& + \left[\frac{7}{4}\cos\gamma_1\sin(\gamma_2+\gamma_3) - \sin\gamma_1\cos(\gamma_2+\gamma_3)\right] \\
& \times \left[\sin(\phi_1-\phi_4)\cos\phi_4 - (\sin\phi_1 - \sin\phi_4)\right]\sin^2\left(\frac{\phi_2-\phi_3}{2}\right)\Bigg\}\hat{\mathbf{x}} \\
& + \frac{1}{2}\Bigg\{ \left[\frac{7}{4}\cos\gamma_3\sin(\gamma_1+\gamma_2) - \sin\gamma_3\cos(\gamma_1+\gamma_2)\right] \\
& \times \left[\sin(\phi_3-\phi_4)\sin\phi_4 + (\cos\phi_3 - \cos\phi_4)\right]\sin^2\left(\frac{\phi_1-\phi_2}{2}\right) \\
& + \left[\frac{7}{4}\cos\gamma_2\sin(\gamma_1+\gamma_3) - \sin\gamma_2\cos(\gamma_1+\gamma_3)\right] \\
& \times \left[\sin(\phi_2-\phi_4)\sin\phi_4 + (\cos\phi_2 - \cos\phi_4)\right]\sin^2\left(\frac{\phi_1-\phi_3}{2}\right) \\
& + \left[\frac{7}{4}\cos\gamma_1\sin(\gamma_2+\gamma_3) - \sin\gamma_1\cos(\gamma_2+\gamma_3)\right] \\
& \times \left[\sin(\phi_1-\phi_4)\sin\phi_4 + (\cos\phi_1 - \cos\phi_4)\right]\sin^2\left(\frac{\phi_2-\phi_3}{2}\right)\Bigg\}\hat{\mathbf{y}} \\
& + \Bigg\{ \left[\frac{7}{4}\sin\gamma_3\sin(\gamma_1+\gamma_2) + \cos\gamma_3\cos(\gamma_1+\gamma_2)\right] \\
& \quad \times \sin^2\left(\frac{\phi_3-\phi_4}{2}\right)\sin^2\left(\frac{\phi_1-\phi_2}{2}\right) \\
& + \left[\frac{7}{4}\sin\gamma_2\sin(\gamma_1+\gamma_3) + \cos\gamma_2\cos(\gamma_1+\gamma_3)\right] \\
& \quad \times \sin^2\left(\frac{\phi_2-\phi_4}{2}\right)\sin^2\left(\frac{\phi_1-\phi_3}{2}\right) \\
& + \left[\frac{7}{4}\sin\gamma_1\sin(\gamma_2+\gamma_3) + \cos\gamma_1\cos(\gamma_2+\gamma_3)\right] \\
& \quad \times \sin^2\left(\frac{\phi_1-\phi_4}{2}\right)\sin^2\left(\frac{\phi_2-\phi_3}{2}\right)\Bigg\}\hat{\mathbf{z}} \qquad \text{(A1)}
\end{aligned}
$$

[1] D. R. Yennie, Precision tests of QED, AIP Conference Proceedings **123**, 468 (1984).

[2] R. Escribano and E. Massó, High precision tests of QED and physics beyond the standard model, Eur. Phys. J. C **4**, 139 (1998).

[3] A. Gumberidze, T. Stöhlker, D. Banaś, K. Beckert, P. Beller, H. F. Beyer, F. Bosch, X. Cai, S. Hagmann, C. Kozhuharov, D. Liesen, F. Nolden, X. Ma, P. H. Mokler, M. Steck, D. Sierpowski, S. Tashenov, A. Warczak, and Y. Zou, Precision tests of QED in strong fields: experiments on hydrogen- and helium-like uranium, J. Phys.: Conf. Ser. **58**, 87 (2007).

[4] J. S. Heyl and L. Hernquist, Birefringence and dichroism of the QED vacuum, J. Phys. A: Math. Gen. **30**, 6485 (1997).

[5] J. J. Klein and B. P. Nigam, Birefringence of the Vacuum, Phys. Rev. **135**, B1279 (1964), publisher: American Physical Society.

[6] T. Heinzl, B. Liesfeld, K.-U. Amthor, H. Schwoerer, R. Sauerbrey, and A. Wipf, On the observation of vacuum birefringence, Optics Communications **267**, 318 (2006).

[7] F. Karbstein, C. Sundqvist, K. S. Schulze, I. Uschmann, H. Gies, and G. G. Paulus, Vacuum birefringence at x-ray free-electron lasers, New Journal of Physics **23**, 095001 (2021).

[8] R. P. Mignani, V. Testa, D. González Caniulef, R. Taverna, R. Turolla, S. Zane, and K. Wu, Evidence for vacuum birefringence from the first optical-polarimetry measurement of the isolated neutron star RX J1856.53754, Monthly Notices of the Royal Astronomical Society **465**, 492 (2016), https://academic.oup.com/mnras/article-pdf/465/1/492/8593962/stw2798.pdf.

[9] V. Denisov, E. Dolgaya, and V. Sokolov, Nonperturbative QED vacuum birefringence, J. High Energ. Phys. **2017** (5), 105.

[10] M. Formanek, J. P. Palastro, D. Ramsey, S. Weber, and A. Di Piazza, Signatures of vacuum birefringence in low-power flying focus pulses, Phys. Rev. D **109**, 056009 (2024).

[11] T. N. Wistisen and U. I. Uggerhøj, Vacuum birefringence by compton backscattering through a strong field, Phys. Rev. D **88**, 053009 (2013).

[12] F. Karbstein, H. Gies, M. Reuter, and M. Zepf, Vacuum birefringence in strong inhomogeneous electromagnetic fields, Phys. Rev. D **92**, 071301 (2015).

[13] A. Ejlli, F. Della Valle, U. Gastaldi, G. Messineo, R. Pengo, G. Ruoso, and G. Zavattini, The pvlas experiment: A 25 year effort to measure vacuum magnetic birefringence, Physics Reports **871**, 1 (2020), the PVLAS experiment: A 25 year effort to measure vacuum magnetic birefringence.

[14] R. Baier and P. Breitenlohner, The vacuum refraction index in the presence of external fields, Nuovo Cimento B (1965-1970) **47**, 117 (1967).

[15] W. Becker and H. Mitter, Vacuum polarization in laser fields, Journal of Physics A: Mathematical and General **8**, 1638 (1975).

[16] D. M. Tennant, Four wave mixing as a probe of the vacuum, Phys. Rev. D **93**, 125032 (2016).

[17] J. Lundin, M. Marklund, E. Lundström, G. Brodin, J. Collier, R. Bingham, J. T. Mendonça, and P. Norreys, Analysis of four-wave mixing of high-power lasers for the detection of elastic photon-photon scattering, Phys. Rev. A **74**, 043821 (2006).

[18] E. Lundström, G. Brodin, J. Lundin, M. Marklund, R. Bingham, J. Collier, J. T. Mendonça, and P. Norreys, Using High-Power Lasers for Detection of Elastic Photon-Photon Scattering, Phys. Rev. Lett. **96**, 083602 (2006), publisher: American Physical Society.

[19] B. King, H. Hu, and B. Shen, Three-pulse photon-photon scattering, Phys. Rev. A **98**, 023817 (2018).

[20] F. Moulin and D. Bernard, Four-wave interaction in gas and vacuum: definition of a third-order nonlinear effective susceptibility in vacuum: vacuum(3), Optics Communications **164**, 137 (1999).

[21] A. J. Macleod and B. King, Fundamental constants from photon-photon scattering in three-beam collisions 10.48550/arXiv.2406.10342 (2024), arXiv:2406.10342 [hep-ph, physics:physics].

[22] R. Aboushelbaya, K. Glize, A. Savin, M. Mayr, B. Spiers, R. Wang, J. Collier, M. Marklund, R. Trines, R. Bingham, and P. Norreys, Orbital Angular Momentum Coupling in Elastic Photon-Photon Scattering, Phys. Rev. Lett. **123**, 113604 (2019), publisher: American Physical Society.

[23] K. Homma, Sensitivity to dark energy candidates by searching for four-wave mixing of high-intensity lasers in the vacuum, Progress of Theoretical and Experimental Physics **2012**, 04D004 (2012), https://academic.oup.com/ptep/article-pdf/2012/1/04D004/11597538/pts073.pdf.

[24] P. Böhl, B. King, and H. Ruhl, Vacuum high-harmonic generation and electromagnetic shock, Journal of Plasma Physics **82**, 655820202 (2016), publisher: Cambridge University Press.

[25] V. N. Baier, A. I. Milstein, and R. Z. Shaisultanov, Photon Splitting in a Very Strong Magnetic Field, Phys. Rev. Lett. **77**, 1691 (1996), arXiv:hep-th/9604028.

[26] S. L. Adler, Photon splitting and photon dispersion in a strong magnetic field, Annals of Physics **67**, 599 (1971).

[27] A. Di Piazza, K. Z. Hatsagortsyan, and C. H. Keitel, Laser photon merging in proton-laser collisions, Phys. Rev. A **78**, 062109 (2008), arXiv:0906.5576 [hep-ph].

[28] H. Gies, F. Karbstein, and R. Shaisultanov, Laser photon merging in an electromagnetic field inhomogeneity, Phys. Rev. D **90**, 033007 (2014), arXiv:1406.2972 [hep-ph, physics:quant-ph].

[29] H. Gies, F. Karbstein, and N. Seegert, Photon merging and splitting in electromagnetic field inhomogeneities, Phys. Rev. D **93**, 085034 (2016), arXiv:1603.00314 [hep-ph, physics:hep-th, physics:quant-ph].

[30] H. Gies, F. Karbstein, and N. Seegert, Quantum reflection as a new signature of quantum vacuum nonlinearity, New J. Phys. **15**, 083002 (2013).

[31] D. L. Burke, R. C. Field, G. Horton-Smith, J. E. Spencer, D. Walz, S. C. Berridge, W. M. Bugg, K. Shmakov, A. W. Weidemann, C. Bula, K. T. McDonald, E. J. Prebys, C. Bamber, S. J. Boege, T. Koffas, T. Kotseroglou, A. C. Melissinos, D. D. Meyerhofer, D. A. Reis, and W. Ragg, Positron production in multiphoton light-by-light scattering, Phys. Rev. Lett. **79**, 1626 (1997).

[32] M. Aaboud, G. Aad, B. Abbott, and et al., Evidence for light-by-light scattering in heavy-ion collisions with the atlas detector at the lhc, Nature Physics **13**, 852–858 (2017).

[33] G. Aad, B. Abbott, D. C. Abbott, and et al., Observation and measurement of forward proton scattering in association with lepton pairs produced via the photon fusion mechanism at atlas, Physical Review Letters **125**, 10.1103/physrevlett.125.261801 (2020).

[34] M. Marklund and J. Lundin, Quantum vacuum experiments using high intensity lasers, Eur. Phys. J. D **55**, 319 (2009).

[35] S. Robertson, A. Mailliet, X. Sarazin, F. Couchot, E. Baynard, J. Demailly, M. Pittman, A. Djannati-Ataï, S. Kazamias, and M. Urban, Experiment to observe an optically induced change of the vacuum index, Phys. Rev. A **103**, 023524 (2021), publisher: American Physical Society.

[36] N. Ahmadiniaz, C. Bähtz, A. Benediktovitch, and et al., Letter of Intent: Towards a Vacuum Birefringence Experiment at the Helmholtz International Beamline for Extreme Fields (2024), arXiv:2405.18063 [hep-ex, physics:hep-ph, physics:physics].

[37] K. A. Tanaka, K. M. Spohr, D. L. Balabanski, S. Balascuta, L. Capponi, M. O. Cernaianu, M. Cuciuc,

A. Cucoanes, I. Dancus, A. Dhal, B. Diaconescu, D. Doria, P. Ghenuche, D. G. Ghita, S. Kisyov, V. Nastasa, J. F. Ong, F. Rotaru, D. Sangwan, P.-A. Söderström, D. Stutman, G. Suliman, O. Tesileanu, L. Tudor, N. Tsoneva, C. A. Ur, D. Ursescu, and N. V. Zamfir, Current status and highlights of the ELI-NP research program, Matter and Radiation at Extremes **5**, 024402 (2020), https://pubs.aip.org/aip/mre/article-pdf/doi/10.1063/1.5093535/15750185/024402_1_online.pdf.

[38] C. Hernandez-Gomez, Vulcan 20-20 upgrade, `https://www.clf.stfc.ac.uk/Pages/Vulcan-2020.aspx`.

[39] Z. J., Ep-opal – planning for a next-generation laser user facility dedicated to the study of ultra-high intensity laser-matter interactions (2023), `https://indico.duke.edu/event/1/contributions/60/`.

[40] Flagship experiment selection report (2024), `https://nsf-opal.rochester.edu`.

[41] X. Wang, X. Liu, X. Lu, and et al., 13.4 fs, 0.1 hz opcpa front end for the 100 pw-class laser facility, Ultrafast Science **2022** (2022).

[42] M. Born and L. Infeld, Foundations of the New Field Theory, Proceedings of the Royal Society of London. Series A, Containing Papers of a Mathematical and Physical Character **144**, 425 (1934), publisher: The Royal Society.

[43] A. Dehghani, M. R. Setare, and S. Zarepour, Self-energy problem, vacuum polarization, and dual symmetry in Born-Infeld-type $U(1)$ gauge theories, Eur. Phys. J. Plus **137**, 859 (2022), arXiv:2112.03757 [hep-th].

[44] S. Villalba-Chávez and A. Di Piazza, Axion-induced birefringence effects in laser driven nonlinear vacuum interaction, J. High Energ. Phys. **2013** (11), 136, arXiv:1307.7935 [hep-ph, physics:physics].

[45] J. M. A. Paixão, L. P. R. Ospedal, M. J. Neves, and J. A. Helayël-Neto, Probing the interference between non-linear, axionic and space-time-anisotropy effects in the QED vacuum, J. High Energ. Phys. **2024** (5), 29, arXiv:2303.10162 [hep-th, physics:physics].

[46] H. Gies, J. Jaeckel, and A. Ringwald, Polarized Light Propagating in a Magnetic Field as a Probe for Millicharged Fermions, Phys. Rev. Lett. **97**, 140402 (2006), publisher: American Physical Society.

[47] A. Lindner, B. Ölmez, and H. Ruhl, Numerical Simulations of the Nonlinear Quantum Vacuum in the Heisenberg-Euler Weak-Field Expansion, Journal of Computational Physics: X **17**, 100124 (2023), arXiv:2109.08121 [physics].

[48] H. Gies, F. Karbstein, and C. Kohlfürst, All-optical signatures of Strong-Field QED in the vacuum emission picture, Phys. Rev. D **97**, 036022 (2018), arXiv:1712.03232 [hep-ph, physics:hep-th, physics:quant-ph].

[49] T. Grismayer, R. Torres, P. Carneiro, F. Cruz, R. A. Fonseca, and L. O. Silva, Quantum Electrodynamics vacuum polarization solver, New J. Phys. **23**, 095005 (2021), publisher: IOP Publishing.

[50] R. A. Fonseca, L. O. Silva, F. S. Tsung, V. K. Decyk, W. Lu, C. Ren, W. B. Mori, S. Deng, S. Lee, T. Katsouleas, and J. C. Adam, enOSIRIS: A Three-Dimensional, Fully Relativistic Particle in Cell Code for Modeling Plasma Based Accelerators, in en*Computational Science — ICCS 2002*, Vol. 2331, edited by G. Goos, J. Hartmanis, J. Van Leeuwen, P. M. A. Sloot, A. G. Hoekstra, C. J. K. Tan, and J. J. Dongarra (Springer Berlin Heidelberg, Berlin, Heidelberg, 2002) pp. 342–351, series Title: Lecture Notes in Computer Science.

[51] T. Grismayer, M. Vranic, J. L. Martins, R. A. Fonseca, and L. O. Silva, EnglishLaser absorption via quantum electrodynamics cascades in counter propagating laser pulses, Physics of Plasmas **23**, 056706 (2016).

[52] T. Grismayer, M. Vranic, J. L. Martins, R. A. Fonseca, and L. O. Silva, EnglishSeeded QED cascades in counterpropagating laser pulses, Physical Review E **95**, 1135 (2017).

[53] Óscar Amaro, C. Badiali, and B. Martinez, Neural network sampling of bethe-heitler process in particle-in-cell codes (2024), arXiv:2406.02491 [physics.comp-ph].

[54] W. Heisenberg and H. Euler, deFolgerungen aus der Diracschen Theorie des Positrons, Z. Physik **98**, 714 (1936).

[55] J. Schwinger, On Gauge Invariance and Vacuum Polarization, Phys. Rev. **82**, 664 (1951), publisher: American Physical Society.

[56] G. V. Dunne and T. M. Hall, Borel summation of the derivative expansion and effective actions, Phys. Rev. D **60**, 065002 (1999), publisher: American Physical Society.

[57] M. Soljačić and M. Segev, Self-trapping of electromagnetic beams in vacuum supported by QED nonlinear effects, Phys. Rev. A **62**, 043817 (2000), publisher: American Physical Society.

[58] R. P. T. Torres, *Realistic modelling of vacuum polarization induced light scattering scenarios in extreme intense fields*, Master's thesis (2017).

[59] N. Ahmadiniaz, T. Cowan, R. Sauerbrey, U. Schramm, H.-P. Schlenvoigt, and R. Schützhold, Heisenberg limit for detecting vacuum birefringence, Physical Review D **101**, 10.1103/physrevd.101.116019 (2020).

[60] E. Lundstrom, *Detection of elastic photon-photon scattering through four-wave coupling*, Ph.D. thesis, arXiv (2005), arXiv:hep-ph/0512033.

[61] K. Yee, Numerical solution of initial boundary value problems involving maxwell's equations in isotropic media, IEEE Transactions on Antennas and Propagation **14**, 302 (1966).

[62] T. D. Arber, K. Bennett, C. S. Brady, A. Lawrence-Douglas, M. G. Ramsay, N. J. Sircombe, P. Gillies, R. G. Evans, H. Schmitz, A. R. Bell, and C. P. Ridgers, Contemporary particle-in-cell approach to laser-plasma modelling, Plasma Phys. Control. Fusion **57**, 113001 (2015), publisher: IOP Publishing.

[63] R. R. de Almeida, por*Arbitrarily non-paraxial electromagnetic wave-packets in particle-in-cell codes*, Master's thesis (2023).

[64] F. Pampaloni and J. Enderlein, Gaussian, hermite-gaussian, and laguerre-gaussian beams: A primer (2004), arXiv:physics/0410021 [physics.optics].